THE JOURNAL OF PHYSICAL CHEMISTRY LETTERS
A JOURNAL OF THE AMERICAN CHEMICAL SOCIETY

pubs.acs.org/JPCL

Letter

Interplay between Epitaxial Growth and Spin-Crossover Properties of Molecular Ultrathin Films on Metallic Surface

Amandine Bellec,* Tanuja Shridhar Joshi, Ritam Chakraborty, Yves Garreau, Massine Kelai, Lalminthang Kipgen, Talal Mallah, Marie-Laure Boillot, Marie-Anne Arrio, Edwige Otero, Vincent Repain, Shobhana Narasimhan, and Alessandro Coati

Cite This: *J. Phys. Chem. Lett.* 2026, 17, 5223−5230

Read Online

ACCESS | Metrics & More | Article Recommendations | Supporting Information

ABSTRACT: For their incorporation in molecular spintronic devices, it is mandatory to understand how the properties of spin-crossover molecules are modified when they are in direct contact with metallic substrates and how the growth of molecular films is governed by the substrate. In this context, we investigate in detail the structure of $[Fe^{II}(HB(3,5\text{-}(CH_3)_2Pz)_3)_2]$ (Pz = pyrazolyl) ultrathin films adsorbed on Cu(110) using grazing incidence X-ray diffraction measurements, along with their spin-crossover properties measured by X-ray absorption spectroscopy. For submonolayer coverage, the molecules self-assemble into two equivalent domains that are in a perfect epitaxial relationship with the Cu(110) substrate at room temperature. In parallel, the molecules are fully locked in a high spin (HS) state at low temperature. Density functional theory calculations show that there is a complex interplay between the epitaxial strain effect and the binding to the substrate that governs the orientation growth and the spin-crossover properties of the molecular films. For thicker thicknesses, a layer-by-layer growth of the (100) planes of the molecular bulk crystal with the release of the epitaxial constraint is observed, while the spin-crossover properties of the films are partially recovered with the opening of a hysteresis. The results obtained are very different from those observed on thin films adsorbed on Cu(111), indicating that not only the nature of the substrate but also its symmetry influences the spin-crossover properties of molecules.

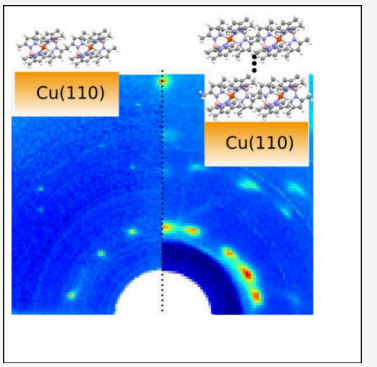

Spin-crossover molecules are promising candidates in the field of molecular electronics and spintronics,[1−4] as they present two spin states that can be addressed by external stimuli. In the solid state, the polymorphism of the molecular crystals has strong consequences regarding the switchability of the spin state of the material.[5,6] For their incorporation in future devices, a fundamental understanding of the spin-crossover properties of molecular films in contact with substrates is needed.[7−9] When the material is in the form of a film, different phases can also be observed, which might or might not present spin-crossover properties.[10−12] Thus, the structure of the molecular film must also be considered. The determination of the structures of molecular ultrathin films (less than a few nanometers) and of the associated interface with the substrate is scarce in the literature and has mainly consisted of analysis by atomic force microscopy to determine the morphology of the films.

In real space, at the molecular level, the adsorption geometry of the molecules on model conducting substrates can be determined by using scanning tunneling microscopy along with the spin-crossover properties. For $[Fe(1,10\text{-phenanthroline})_2(NCS)_2]$ molecules, regardless of the symmetry of the metallic substrate, the molecules are adsorbed in a mixture of molecules in high spin (HS) and low spin (LS) states due to the chemisorption.[13,14] In such a strongly coupled system, only the use of decoupling layers, such as nitrogen or a molecular layer, enables a partial recovery of the spin-crossover properties.[14,15] Interestingly, when deposited directly on an Ag(111) metallic substrate, $Fe(H_2B(pyrazole)(pyridyl\text{-}pyrazole))_2$ molecules form tetramers composed of two molecules that can switch from one spin state to the other, while spin-crossover in the other two molecules is blocked due to steric interactions,[16] emphasizing once again the importance of the molecular environment.

Concerning the interface, studies on various systems have revealed that the nature of the substrate plays an important role in the spin conversion, with a better completeness on substrates with lower electronic density at the Fermi level, such as graphite or semiconducting substrates.[17−21] The influence of the epitaxial relationship between the molecular layer and the underlying substrate is also of paramount importance, both for the growth of a specific molecular crystalline phase and for the spin-crossover properties.[22,23] This means that not only the

Received: February 16, 2026
Revised: April 7, 2026
Accepted: April 10, 2026
Published: April 22, 2026

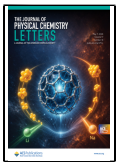

https://doi.org/10.1021/acs.jpclett.6c00550
J. Phys. Chem. Lett. 2026, 17, 5223−5230

nature of the substrate but also the crystallographic parameters of its surface can be important.

In this paper, we show by measuring a model molecule on Cu(110) that indeed its behavior is very different compared to that found on Cu(111). To do this, we have focused our study on thin films of $[Fe^{II}((3,5\text{-}(CH_3)_2Pz)_3BH)_2]$ (Pz = pyrazolyl, called FeMPz in the following) grown on Cu(110), which presents a rectangular symmetry. The structure of molecular spin-crossover films from submonolayer coverage to a few layers thick has been investigated in detail, as well as their spin state switching properties while varying the temperatures. Using X-ray absorption (XA) spectroscopy, we observed that the thermal spin-crossover transition is strongly modified compared to what is observed for deposition on a Cu(111) substrate[23] and that for different molecular film thicknesses. By grazing incidence X-ray diffraction (GIXD) at room temperature, we carried out a structural study of ultrathin molecular films of various thicknesses to understand their growth. We observed a strong epitaxial relationship between the molecular film and the substrate for submonolayer coverage, presenting only two molecular domains. Complementary DFT calculations underline the importance of both the epitaxial strain and the molecule−substrate interaction for the spin-crossover properties. For higher coverages, the structure of the molecular film evolves to release the constraint imposed by the epitaxy, and the film is composed of (100) planes with respect to the molecular bulk structure.

First, the spin-crossover properties of the molecular ultrathin films on Cu(110) have been probed by X-ray absorption spectroscopy. Figure 1a,b shows the spectra measured at room temperature and low temperature (300 and 4 K, respectively) for 1.0 ± 0.3 and 5.9 ± 1.5 ML films, respectively. For both thicknesses, the spectra at room temperature (black curves in Figure 1a,b) are typical of the FeMPz molecules in the HS state.[23] Upon reducing the temperature to 4 K, for the 1 ML film, the proportion of molecules in the HS state remains constant, the spectrum modifications observed being only due to the variation of the Boltzmann repartition with the temperature in the HS initial states.[23] On the contrary, for the 5.9 ML film, the shape of the spectrum evolves due to the HS-to-LS conversion of some molecules. Quantitatively, for the 5.9 ML film, the proportion of molecules in the HS state decreases with decreasing temperature, from 100% at 300 K to 49 ± 3% at 4 K (see the Supporting Information (SI) and Figure S1). To characterize the thermal transition over the whole temperature range, we extracted from the XA spectra the proportion of molecules in the HS state as a function of temperature while ramping the temperature up and down (sweeping ramp of 1.25 K·min^{-1}). As shown in Figure 1c, the molecules are completely locked in HS states for the 1.0 ML film on Cu(110), whereas when grown on Cu(111), a partial conversion is observed.[23] For the 5.9 ML film, the conversion is partial, and a small hysteresis of 14 ± 8 K is observed. The width of the hysteresis is smaller than the width measured for the bulk[10] or ultrathin films grown on Cu(111),[23] but it confirms the existence of hysteresis in ultrathin films. In the framework of the mechano-elastic model,[23,24] the evolution of the width observed between the (110) and (111) orientations of Cu could be described by the variation of interaction with the substrate. These XA measurements indicate that not only the nature of the metallic substrate[19,23,25,26] but also its symmetry has an influence on the molecular spin-crossover properties. To understand how the symmetry of the substrate

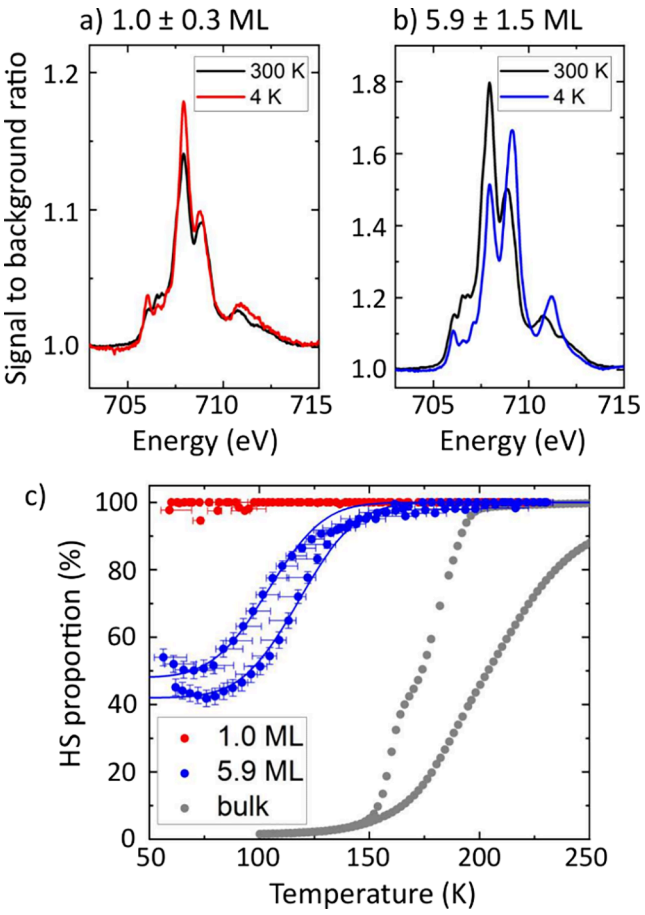

Figure 1. XA spectra at the Fe L_3-edge at room temperature (black curves) and low temperature (4 K, colored curves) for a molecular film of (a) 1.0 ± 0.3 and (b) 5.9 ± 1.5 ML. The absorption is plotted as the signal to background ratio so that the percentage of the edge jump can be read directly. (c) Evolution of the percentage of molecules in the HS state, extracted from the XA spectra, as a function of temperature, for a sweeping ramp of 1.25 K·min^{-1} for the 1.0 ± 0.3 (red dots) and 5.9 ± 1.5 ML (blue dots) films. The percentage of HS state molecules in the bulk is added as gray points (extracted from SQUID measurements, sweeping ramp of 2 K·min^{-1}).

impacts the grown molecular layer, we investigated in detail the structure of the molecular film at room temperature as well as its relationship to the Cu(110) substrate for various film thicknesses.

Figure 2a shows the in-plane (h, k) map obtained by GIXD measurements for a submonolayer of FeMPz molecules adsorbed on Cu(110). All of the diffraction measurements are presented using the orthogonal basis linked to the Cu(110) surface for which $\vec{a}^*_{Cu(110)}$ and $\vec{b}^*_{Cu(110)}$ are schematized by orange arrows in the map in Figure 2a (see the Methods section for more details). The intense peaks at (1, 0), (0, 1), (−1, 0) and (0, −1) correspond to the (h, k) positions of Bragg peaks of the Cu(110) substrate. Other intense spots corresponding to molecular lattices are observed at (h, k) values smaller than 1. Two domains, equivalent by mirror symmetry, can be defined with the $\vec{a}^*_{sub}$ and $\vec{b}^*_{sub}$ lattice parameters schematized by the black and red arrows on the map. The expected positions of the Bragg peaks of the molecular crystal are also indicated by black and red circles. As can be seen by the coincidence of the spots between the

https://doi.org/10.1021/acs.jpclett.6c00550
J. Phys. Chem. Lett. 2026, 17, 5223−5230

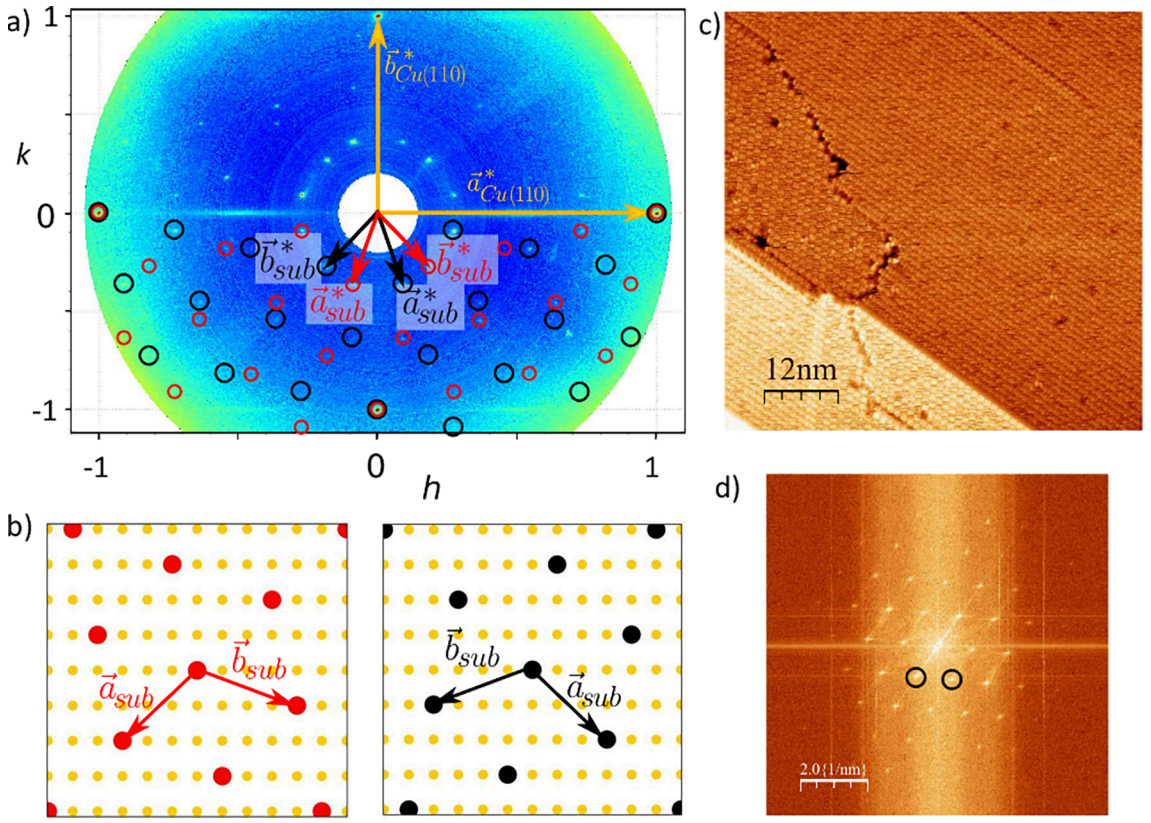

Figure 2. Submonolayer coverage of FeMPz on Cu(110). (a) In-plane (h, k) map (the intensity is integrated along the l-direction in the range 0.05−0.15). The Cu(110) lattice is highlighted by orange arrows; the two molecular domains are highlighted by red and black arrows and circles. (b) Schematic drawings of the epitaxial relationship between the molecular films (red dots on the left and black dots on the right) and the Cu(110) substrate (orange dots). (c) STM topographic image acquired at room temperature (60 × 60 nm^2, V_{bias} = −1.5 V, I_t = 20 pA). (d) Fourier transform of the STM image on which one of the molecular domains is clearly identified (black circles).

molecular domains and the Cu(110) network, the two molecular domains are in perfect registry with the substrate. The epitaxial relationship is defined for the red domain as $\begin{pmatrix} a^*_{Cu(110)} \\ b^*_{Cu(110)} \end{pmatrix} = \begin{pmatrix} -3 & 4 \\ -2 & -1 \end{pmatrix} \begin{pmatrix} a^*_{sub} \\ b^*_{sub} \end{pmatrix}$ The molecular lattice parameters are determined to be $\|\vec{a}_{sub}\|$ = 10.54 Å, $\|\vec{b}_{sub}\|$ = 10.84 Å, and $(\vec{a}_{sub}, \vec{b}_{sub})$ = 117.2°. Figure 2b presents the corresponding schematic drawings in real space of both molecular lattices in an epitaxial relationship with the substrate. The formation of well ordered domains is confirmed by scanning tunneling microscopy (STM) imaging (Figure 2c). For deposition at room temperature, the molecules self-assemble in domains with a size of around 40 nm (see SI and Figure S2). The Fourier transform of the STM image (Figure 2d) shows one of the domain orientations compatible with GIXD measurements.

The lattice parameters of the epitaxial domain can be compared to those expected for various dense planes of the bulk molecular crystal for the high spin phase.[10] Interestingly, they are quite close to the lattice parameters describing the (100) plane of the molecular bulk, whose values are $\|\vec{B}_{(100)}\|$ = 10.22 Å, $\|\vec{C}_{(100)}\|$ = 10.79 Å, and $\alpha_{(100)}$ = 116.4°. In comparison to the bulk plane, the epitaxial molecular film is constrained by 3.2% along the direction of $\vec{a}_{sub}$ and by 0.5% along the direction of $\vec{b}_{sub}$. Interestingly, the molecular structure of the monolayer film on Cu(110) is different from the one obtained on Au(111)[22] and Cu(111).[27]

To confirm and interpret the experimental results, we have performed spin-polarized density functional theory (DFT) calculations using the Quantum ESPRESSO package.[28,29] In these calculations, exchange correlation interactions were treated using the PBE form of the Generalized Gradient Approximation,[30] and van der Waals interactions were incorporated using the DFT-D3 method.[31] Strong correlations were treated using Hubbard parameter U = 2 eV on Fe d orbitals.[32] Further details justifying the choice of U and other calculation details can be found in the Supporting Information (see the SI, Figure S3, and Table S1).

We first calculate the surface energies of different facets of the bulk HS molecular crystal, namely the dense facets (100), (01$\bar{1}$), (010), and (001). We find that the facet with the lowest surface energy is (01$\bar{1}$), as can be seen from the results presented in Table 1. This suggests that it is not the surface energy alone that primarily governs the favored molecular

Table 1. DFT Results for the Surface Energy (σ) of the Molecular Crystal and the Adsorption Energy (E_{ads}) for One Monolayer Adsorbed on Cu(110), for the Four Orientations of the Molecular Crystal Investigated

	(100)	(01$\bar{1}$)	(010)	(001)
σ (meV·Å^{-2})	3.801	3.707	3.838	4.600
E_{ads} (eV)	−2.320	−2.231	−2.094	−1.494

https://doi.org/10.1021/acs.jpclett.6c00550
J. Phys. Chem. Lett. 2026, 17, 5223−5230

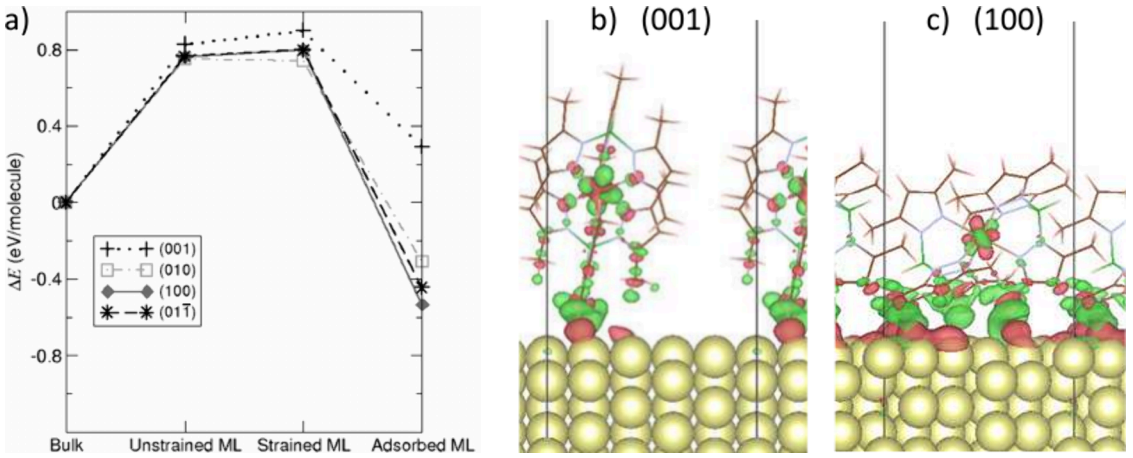

Figure 3. (a) Variation of the total energy with respect to the bulk for the four different orientations considered (ΔE), as one goes from the bulk molecular crystal to the monolayer on the substrate in three steps: (i) carving out the monolayer from the bulk crystal, (ii) straining the monolayer to obtain lattice-matching with the substrate, and (iii) depositing the strained monolayer on the substrate. Adsorption geometries and charge redistribution for the molecular film orientations of (b) (001) and (c) (100) on the Cu(110) substrate. The charge redistribution ($\Delta\rho$) is plotted using an isosurface value of $\pm 5 \times 10^{-4}$ e/bohr^3. The red and green lobes represent regions of electron accumulation and depletion, respectively. The FeMPz is visualized as a wireframe, and the pale yellow spheres correspond to Cu atoms. The vertical black lines show the boundaries of a surface unit cell. High spin state is assumed in the structural model.

orientation on the Cu(110) substrate. Previous theoretical attempts to understand the formation of low-dimensional SCO materials on substrates have relied on semiempirical models that are used to separate out contributions from surface energy, surface stress, and interface stress.[2,24,33,34] Here, we instead adopt a novel perspective using only first-principles calculations and perform a thought experiment in which the formation of a self-assembled monolayer is conceptually separated into three steps. In the first step, a (*hkl*) monolayer is carved out from bulk FeMPz in the high spin state. Next, the freestanding (*hkl*) monolayer is strained to the lattice parameters it will have when deposited on the substrate with an epitaxial relationship (see the SI and Table S2). We note that these lattice parameters match the experiment best for the (100) orientation. Finally, the strained (*hkl*) monolayer is deposited on the substrate. Figure 3a shows how the total energy changes with respect to the bulk as the system changes from the bulk to the freestanding monolayer, then to the strained monolayer, and finally to the adsorbed one for the four different molecular orientations considered. After the first step, the molecular (010) orientation is the lowest in energy, and this remains true when the molecular layer is strained in the second step. However, after adsorption on Cu(110), the (100) orientation becomes the lowest energy geometry. Thus, both the supercell geometry and the DFT energetics support that the FeMPz is deposited on Cu(110) with the orientation that it has in the (100) plane of the bulk molecular crystal. These results also suggest that it is primarily molecule–substrate binding, rather than epitaxial strain, that determines the adsorption geometry. The relaxed adsorption geometries along with the isosurfaces of the charge redistribution are shown in Figure 3b,c for the (001) and the (100) planes, respectively (the adsorption geometries for the other orientations can be found in Figure S4 in the SI). The charge redistribution that occurs when the monolayer is deposited on the substrate is defined as $\Delta\rho = \rho_{ml/sub} - \rho_{ml} - \rho_{sub}$, where $\rho_{ml/sub}$, ρ_{ml}, and ρ_{sub} are the charge densities of the monolayer on the substrate, the monolayer alone, and the bare substrate, respectively. In Figure 3b,c, the red and green lobes represent regions of charge accumulation and depletion, respectively. Alternating green and red lobes indicate a bond formed between the monolayer and the substrate, and the size of these lobes is an indication of the strength of the bond. By visual comparison (Figure 3b,c), we can see that the number and strength of the bonds are greatest in the (100) orientation and lowest in the (001) orientation. To understand the reason for this, we note that the number of H atoms available to form such bonds varies with the molecular orientation. A greater number of hydrogen atoms that are close to the substrate (e.g., within a distance of 3 Å from the topmost layer of the substrate) is available in the case of the (100) orientation compared to the others, thus explaining the stronger adsorption (see Figure S5 in the SI). Thus, we conclude that the important parameter that governs the epitaxial growth of FeMPz on Cu(110) is the interaction with the substrate via the bonds between the peripheral H atoms in FeMPz and the substrate. We also use DFT to compute the difference in total energy between the high and low spin configurations (ΔE_{HL}). For the bulk molecular crystal, ΔE_{HL} = 102 meV. For an unstrained (100) monolayer, ΔE_{HL} = 150 meV. For the strained (100) monolayer, ΔE_{HL} = 97 meV, and for a (100) monolayer deposited on Cu(110), ΔE_{HL} = 140 meV. These results show that there is a complex interplay between strain effects and binding to the substrate that affects the ΔE_{HL} value. These results alone cannot explain spin locking on Cu(110), as the values of ΔE_{HL} are comparable in the molecular crystal and the monolayer on Cu(110). This may be due to our neglect of entropic contributions to the thermodynamic free energy, which could be quite different (especially the vibrational part) on the surface than in the bulk. Alternatively, the HS state could be kinetically trapped due to a large activation energy barrier for the HS-to-LS transition. We note that strong binding to the substrate is likely to increase this barrier due to the structural transition that accompanies the spin-crossover. Unfortunately, the large system size makes explicit calculations of entropic and kinetic effects infeasible in a reasonable time scale.

https://doi.org/10.1021/acs.jpclett.6c00550
J. Phys. Chem. Lett. 2026, 17, 5223−5230

Upon increasing the molecular film thickness, its structure evolves. Two samples are discussed here, one in the main text and a second in the SI (Figure S6). As visible on the (h, k) map presented in Figure 4, for a 10 ML-thick molecular film,

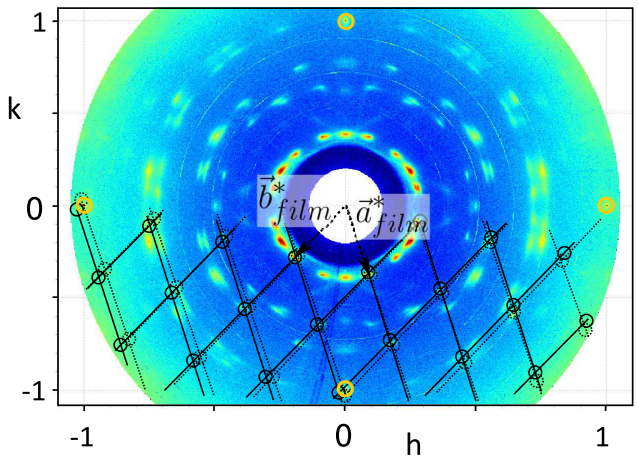

Figure 4. In-plane (h, k) map for the 10 ML-thick molecular film of FeMPz on Cu(110) (the intensity is integrated along the l-direction in the range 0.05−0.15). Two of the nearby molecular lattices ($\vec{a}^*_{film}$ and $\vec{b}^*_{film}$) are highlighted with dashed and solid networks and circles, respectively. The Bragg peak positions of Cu(110) are highlighted by orange circles.

the spots around the positions expected for the epitaxial domains are doubled, and additional spots at intermediate positions corresponding to extra domains are observed. As highlighted by the dashed and solid networks in Figure 4, for a given epitaxial domain, the spots are now doubled, and two misoriented domains with the same lattice parameters (denoted as $\vec{a}_{film}$ and $\vec{b}_{film}$) are observed. For a greater thickness (SI), the same doubling is observed. The determined values of the lattice parameters are $\|\vec{a}_{film}\| = 10.3 \pm 0.1$ Å, $\|\vec{b}_{film}\| = 10.7 \pm 0.1$ Å, and $(\vec{a}_{film}, \vec{b}_{film}) = 117 \pm 1°$. Again, these parameters can be compared to those of the (100) plane of the bulk molecular crystal for the high spin state.[10] Interestingly, with increasing thickness, the lattice parameters evolve to values nearer to those of the (100) plane in the bulk molecular crystal, with the strain imposed being decreased to 0.8% along the direction of $\vec{a}_{film}$ and −0.8% along the direction of $\vec{b}_{film}$. Thus, increasing the thickness of the molecular film leads to relaxation of the epitaxial strain with the doubling of the domains and a growth of (100) molecular planes with respect to the bulk crystal. As detailed in the SI (Figure S7), all of the intermediate spots can be assigned to two domains equivalent by mirror symmetry whose parameters are also similar to those of the (100) plane of the bulk molecular crystal. The thick molecular films are not any more in registry with the substrate, and most probably misfit dislocations or cracks[24] are created in the molecular film near the interface with Cu(110).

Out-of-plane measurements have also been carried out for all of the molecular domains. The intensity along the rods displays modulation with peaks at particular positions (see Figure S8 in the SI). Their positions can be compared to the position expected in l for the Bragg peaks of the bulk molecular crystal exhibiting a (100) plane termination. As detailed in the SI, the agreement between the expected and measured values is very good, thus confirming the growth of the molecular film composed of (100) planes.

In thick molecular films with a thickness of around 20 nm, atomic force microscopy measurements have also been carried out. As can be observed in Figure 5a, the molecular film is composed of flat islands indicating a preferred layer-by-layer growth mode.

Finally, we also performed X-ray reflectivity measurements on the 10 nm-thick FeMPz film grown on Cu(110) and compared the results to those obtained on the bare Cu(110) substrate (see the black dots and green dots, respectively, in Figure 5b). The Bragg peaks of the molecular layer are observed at q_{per} values of 0.782 and 1.486 Å^{-1} and are modulated by Laue oscillations, which indicate that the molecular planes are well-defined. To reproduce these oscillations, we build a model composed of N layers of FeMPz molecules grown on a semi-infinite Cu substrate (see Figure 5c and Figure S9 in the SI). The molecular layers are considered to be (100) planes with respect to the molecular bulk, thus defining the distance between the molecular planes (d_{100}). The best agreement between the simulation (blue curve) and the experimental data is obtained for the d_{100} of the bulk and 10 monolayers of molecules (N = 10). This X-ray

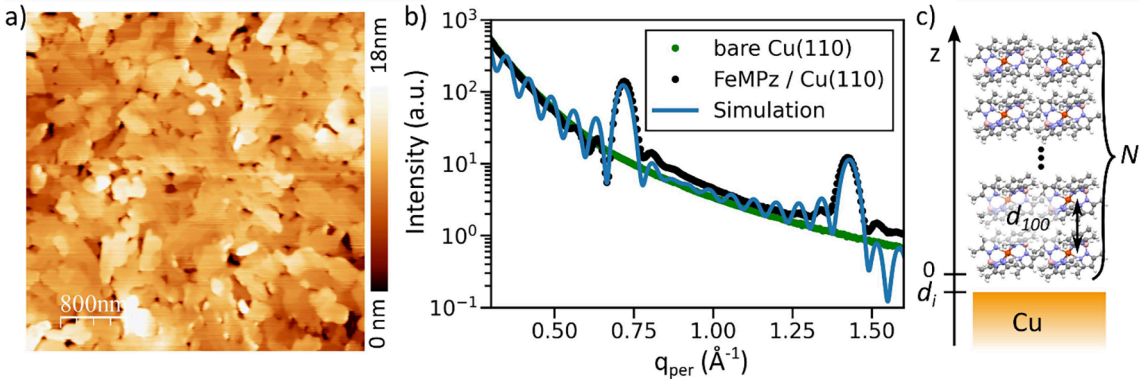

Figure 5. (a) AFM image of a 20 nm-thick molecular film of FeMPz on Cu(110) (4 × 4 μm^2). (b) X-ray reflectivity measurements performed on the 10 nm-thick molecular film of FeMPz on Cu(110) (black dots) and on the bare Cu(110) surface (green dots). The simulated curve is superimposed (blue curve). (c) Schematic drawing of the model developed to simulate reflectivity measurement, considering N FeMPz layers separated by interplanar distance d_{100} and deposited on a Cu semi-infinite crystal.

https://doi.org/10.1021/acs.jpclett.6c00550
J. Phys. Chem. Lett. 2026, 17, 5223−5230

reflectivity measurement confirms that the molecular film is well crystallized and composed of a stack of (100) planes.

To summarize, thin films of FeMPz grow epitaxially in a layer-by-layer mode on Cu(110). For submonolayer coverage, the molecular layer is in perfect epitaxy with the Cu(110), leading to the locking of the molecules in the HS state, as supported by the combination of XA spectroscopy and GIXD measurements. DFT calculations demonstrate that the orientation of the molecular layer is primarily determined by maximizing the molecular−substrate binding, which in turn is determined by the number of peripheral H atoms available to bond with the substrate. The spin state locking cannot be explained by electronic energy differences (ΔE_{HL}) alone; entropic and/or kinetic effects must also be considered. Increasing the molecular coverage leads to the release of the epitaxial constraint in the film and a preferential growth of a molecular film composed of (100) planes with respect to the molecular crystal, and the molecules recover their spin-crossover properties with temperature with the opening of a hysteresis. These results clearly demonstrate that not only the nature of the substrate but also its symmetry plays a role in the spin-crossover properties of molecular films.

METHODS

Sample Preparation

The different samples investigated were prepared under ultrahigh vacuum (UHV, base pressure of 10^{-10} mbar) in different UHV chambers. For all the samples prepared, the Cu(110) single crystal (Surface preparation laboratory, with a purity of 6N) was first cleaned by Ar^+-sputtering (at 1 keV) and annealing (between 500 and 700 °C) cycles. Once the Cu(110) substrate was cleaned, the FeMPz molecules, synthesized following the procedure described by Iasco et al.,[10] were deposited from a homemade evaporator (Knudsen-type) at a crucible temperature around 90 °C. During the molecular deposition, the substrate was kept at room temperature except for the sample measured by STM at low temperature, for which the substrate was kept at 80 K. The coverage of the different samples ranged from submonolayer coverage to around 20 ML. The thickness calibration is further discussed in the SI.

Grazing Incidence X-ray Diffraction

The GIXD experiments were realized on the Surfaces and Interfaces X-ray Scattering (SixS) beamline at synchrotron SOLEIL on the UHV end station.[35] All of the GIXD measurements were performed at room temperature, at a beam energy of 18.4 keV and an incident angle of μ = 0.2°. For the GIXD experiments, the experimental results are presented in the Cu(110) basis, which is defined as follows compared to the fcc structure of Cu: $\vec{a}_{(110)} = \frac{1}{2}[\bar{1}10]$, $\vec{b}_{(110)} = [001]$, and $\vec{c}_{(110)} = \frac{1}{2}[110]$. For the data analysis, binoviewer software was used.[36]

Scanning Probe Microscopy

The submonolayer samples were measured by scanning tunneling microscopy both at low temperature (4.6 K, LT-STM from Omicron Scienta) and at room temperature (VT-XA STM from Omicron Scienta). A thicker sample was imaged by atomic force microscopy (CoreAFM, Nanosurf) using an ultrasharp tip (SSS-NCHR, Nano-AndMore).

X-ray Absorption Spectroscopy

The XA spectroscopy experiments were carried out on the DEIMOS beamline at Synchrotron SOLEIL using total electron yield (TEY) detection.[37] The sample was prepared using a shadow mask during the molecular deposition to define two areas with different thicknesses (1.0 ± 0.3 and 5.9 ± 1.5 ML), which were measured in parallel. Thus, the thermal ramps applied to both thicknesses were exactly the same, and the evolution of the HS proportion as a function of temperature can be directly compared.

DFT Calculations

Density functional theory (DFT) calculations were performed using the Quantum ESPRESSO package.[28,29] The Kohn−Sham orbitals were expanded in a plane wave basis with cutoffs of 60 and 300 Ry for wave functions and charge densities, respectively. We used PAW pseudopotentials,[38] while exchange correlation interactions were treated using the PBE form of the Generalized Gradient Approximation.[30] van der Waals interactions were incorporated using the DFT-D3 method.[31] Strong correlations were described using Hubbard parameter U = 2 eV on Fe d orbitals, following the Dudarev formalism[39] and the subsequent implementation by Cococcioni and de Gironcoli.[32] We fixed the value of the Hubbard parameter U to reproduce the difference in the enthalpy between the LS and HS phases that has been measured to be around 100 meV by calorimetric measurements[10] (see the SI for more details).

ASSOCIATED CONTENT

Supporting Information

The Supporting Information is available free of charge at https://pubs.acs.org/doi/10.1021/acs.jpclett.6c00550.

Determination of the HS proportion from the XA spectra, topographies of the submonolayer FeMPz film, DFT calculations on FeMPz on Cu(110), in-plane map for a thick molecular film, extra domains at intermediate (h, k) positions, out-of-plane measurements, modeling of the Laue oscillations in the reflectivity measurements, and calibration of the molecular film thicknesses (PDF)

AUTHOR INFORMATION

Corresponding Author

Amandine Bellec − *Université Paris Cité, CNRS, Laboratoire Matériaux et Phénomènes Quantiques, F-75013 Paris, France;* orcid.org/0000-0001-7410-9736; Email: amandine.bellec@u-paris.fr

Authors

Tanuja Shridhar Joshi − *Theoretical Sciences Unit and School of Advanced Materials, Jawaharlal Nehru Centre for Advanced Scientific Research, Bangalore 560064, India*

Ritam Chakraborty − *Theoretical Sciences Unit and School of Advanced Materials, Jawaharlal Nehru Centre for Advanced Scientific Research, Bangalore 560064, India*

Yves Garreau − *Université Paris Cité, CNRS, Laboratoire Matériaux et Phénomènes Quantiques, F-75013 Paris, France; Synchrotron SOLEIL, 91190 Saint-Aubin, France*

Massine Kelai − *Université Paris Cité, CNRS, Laboratoire Matériaux et Phénomènes Quantiques, F-75013 Paris, France*

Lalminthang Kipgen − *Université Paris Cité, CNRS, Laboratoire Matériaux et Phénomènes Quantiques, F-75013 Paris, France*

Talal Mallah − *Institut de Chimie Moléculaire et des Matériaux d'Orsay, Université Paris-Saclay, CNRS, UMR 8182, 91405 Orsay, France;* orcid.org/0000-0002-9311-3463

Marie-Laure Boillot − *Institut de Chimie Moléculaire et des Matériaux d'Orsay, Université Paris-Saclay, CNRS, UMR 8182, 91405 Orsay, France;* orcid.org/0000-0001-6710-4523

Marie-Anne Arrio − *CNRS, Sorbonne Université, MNHN, IMPMC, UMR 7509, F-75252 Paris, France;* orcid.org/0000-0002-2945-6824

https://doi.org/10.1021/acs.jpclett.6c00550
J. Phys. Chem. Lett. 2026, 17, 5223−5230

Edwige Otero − *Synchrotron SOLEIL, 91190 Saint-Aubin, France;* orcid.org/0000-0002-3546-3908
Vincent Repain − *Université Paris Cité, CNRS, Laboratoire Matériaux et Phénomènes Quantiques, F-75013 Paris, France*
Shobhana Narasimhan − *Theoretical Sciences Unit and School of Advanced Materials, Jawaharlal Nehru Centre for Advanced Scientific Research, Bangalore 560064, India;* orcid.org/0000-0002-1793-0576
Alessandro Coati − *Synchrotron SOLEIL, 91190 Saint-Aubin, France*

Complete contact information is available at: https://pubs.acs.org/10.1021/acs.jpclett.6c00550

Notes

The authors declare no competing financial interest.

■ ACKNOWLEDGMENTS

We thank Geoffroy Prévôt for sharing with us the software "binoviewer" that he developed for the analysis of GIXD data, Clément Barraud for his help with the AFM measurements, and Aurélie Covasso for assistance with the UHV suitcase. We acknowledge SOLEIL for the provision of synchrotron radiation facilities, and we would like to thank SixS and DEIMOS staff for assistance in using the beamline, especially Benjamin Voisin and Florian Leduc for support with the UHV chamber preparation on SixS and DEIMOS beamlines, respectively. This work was financially supported by the Centre National de la Recherche Scientifique (CNRS, France), the French Ministry of Research and ANR (ANR-21-CE09-0031, 2DSwitch project).

■ REFERENCES

(1) Bellec, A.; Lagoute, J.; Repain, V. Molecular electronics: Scanning tunneling microscopy and single-molecule devices. *Comptes Rendus Chimie* **2018**, *21*, 1287−1299.
(2) Molnár, G.; Rat, S.; Salmon, L.; Nicolazzi, W.; Bousseksou, A. Spin Crossover Nanomaterials: From Fundamental Concepts to Devices. *Adv. Mater.* **2018**, *30*, 1703862.
(3) Lefter, C.; Davesne, V.; Salmon, L.; Molnár, G.; Demont, P.; Rotaru, A.; Bousseksou, A. Charge Transport and Electrical Properties of Spin Crossover Materials: Towards Nanoelectronic and Spintronic Devices. *Magnetochemistry* **2016**, *2*, 18.
(4) Zhang, Y.; Séguy, I.; Soroceanu, I.; Rotaru, A.; Yu, H.; Salmon, L.; Molnár, G.; Bousseksou, A. Integration of the evaporable spin-crossover complex $[Fe(HB(1,2,4\text{-triazol-1-yl})_3)_2]$ into organic field-effect transistors: towards multifunctional OFET devices. *RSC Adv.* **2025**, *15*, 8757−8763.
(5) Tao, J.; Wei, R.-J.; Huang, R.-B.; Zheng, L.-S. Polymorphism in spin-crossover systems. *Chem. Soc. Rev.* **2012**, *41*, 703−737.
(6) Ossinger, S.; Näther, C.; Buchholz, A.; Schmidtmann, M.; Mangelsen, S.; Beckhaus, R.; Plass, W.; Tuczek, F. Spin Transition of an Iron(II) Organoborate Complex in Different Polymorphs and in Vacuum-Deposited Thin Films: Influence of Cooperativity. *Inorg. Chem.* **2020**, *59*, 7966−7979.
(7) Gruber, M.; Berndt, R. Spin-Crossover Complexes in Direct Contact with Surfaces. *Magnetochemistry* **2020**, *6*, 35.
(8) Kipgen, L.; Bernien, M.; Tuczek, F.; Kuch, W. Spin-Crossover Molecules on Surfaces: From Isolated Molecules to Ultrathin Films. *Adv. Mater.* **2021**, *33*, 2008141.
(9) Kumar, K. S.; Ruben, M. Sublimable Spin-Crossover Complexes: From Spin-State Switching to Molecular Devices. *Angew. Chem., Int. Ed.* **2021**, *60*, 7502−7521.
(10) Iasco, O.; Boillot, M.-L.; Bellec, A.; Guillot, R.; Rivière, E.; Mazerat, S.; Nowak, S.; Morineau, D.; Brosseau, A.; Miserque, F.; et al. The disentangling of hysteretic spin transition, polymorphism and metastability in bistable thin films formed by sublimation of bis(scorpionate) Fe(II) molecules. *Journal of Materials Chemistry C* **2017**, *5*, 11067−11075.
(11) Davesne, V.; Gruber, M.; Studniarek, M.; Doh, W. H.; Zafeiratos, S.; Joly, L.; Sirotti, F.; Silly, M. G.; Gaspar, A. B.; Real, J. A.; et al. Hysteresis and change of transition temperature in thin films of $Fe\{[Me_2Pyrz]_3BH\}_2$, a new sublimable spin-crossover molecule. *J. Chem. Phys.* **2015**, *142*, 194702.
(12) Gavara-Edo, M.; Córdoba, R.; Valverde-Muñoz, F. J.; Herrero-Martín, J.; Real, J. A.; Coronado, E. Electrical Sensing of the Thermal and Light-Induced Spin Transition in Robust Contactless Spin-Crossover/Graphene Hybrid Devices. *Adv. Mater.* **2022**, *34*, 2202551.
(13) Gruber, M.; Miyamachi, T.; Davesne, V.; Bowen, M.; Boukari, S.; Wulfhekel, W.; Alouani, M.; Beaurepaire, E. Spin crossover in $Fe(phen)_2(NCS)_2$ complexes on metallic surfaces. *J. Chem. Phys.* **2017**, *146*, No. 092312.
(14) Gruber, M.; Davesne, V.; Bowen, M.; Boukari, S.; Beaurepaire, E.; Wulfhekel, W.; Miyamachi, T. Spin state of spin-crossover complexes: From single molecules to ultrathin films. *Phys. Rev. B* **2014**, *89*, 195415.
(15) Miyamachi, T.; Gruber, M.; Davesne, V.; Bowen, M.; Boukari, S.; Joly, L.; Scheurer, F.; Rogez, G.; Yamada, T. K.; Ohresser, P.; et al. Robust spin crossover and memristance across a single molecule. *Nat. Commun.* **2012**, *3*, 938.
(16) Johannsen, S.; Ossinger, S.; Markussen, T.; Tuczek, F.; Gruber, M.; Berndt, R. Electron-Induced Spin-Crossover in Self-Assembled Tetramers. *ACS Nano* **2021**, *15*, 11770−11778.
(17) Bernien, M.; Naggert, H.; Arruda, L. M.; Kipgen, L.; Nickel, F.; Miguel, J.; Hermanns, C. F.; Krüger, A.; Krüger, D.; Schierle, E.; et al. Highly Efficient Thermal and Light-Induced Spin-State Switching of an Fe(II) Complex in Direct Contact with a Solid Surface. *ACS Nano* **2015**, *9*, 8960−8966.
(18) Kipgen, L.; Bernien, M.; Ossinger, S.; Nickel, F.; Britton, A. J.; Arruda, L. M.; Naggert, H.; Luo, C.; Lotze, C.; Ryll, H.; et al. Evolution of cooperativity in the spin transition of an iron(II) complex on a graphite surface. *Nat. Commun.* **2018**, *9*, 2984.
(19) Rohlf, S.; Grunwald, J.; Jasper-Toennies, T.; Johannsen, S.; Diekmann, F.; Studniarek, M.; Berndt, R.; Tuczek, F.; Rossnagel, K.; Gruber, M. Influence of Substrate Electronic Properties on the Integrity and Functionality of an Adsorbed Fe(II) Spin-Crossover Compound. *J. Phys. Chem. C* **2019**, *123*, 17774−17780.
(20) Ossinger, S.; Kipgen, L.; Naggert, H.; Bernien, M.; Britton, A. J.; Nickel, F.; Arruda, L. M.; Kumberg, I.; Engesser, T. A.; Golias, E.; et al. Effect of ligand methylation on the spin-switching properties of surface-supported spin-crossover molecules. *J. Phys.: Condens. Matter* **2020**, *32*, 114003.
(21) Trapali, A.; Muppal, M.; Pandey, S.; Boillot, M.-L.; Repain, V.; Dappe, Y. J.; Dayen, J.-F.; Rivière, E.; Guillot, R.; Arrio, M.-A.; et al. Investigation of the spin crossover behaviour of a sublimable Fe(II)-qsal complex: from the bulk to a submonolayer on graphene/SiO_2. *Dalton Transactions* **2024**, *53*, 12519.
(22) Fourmental, C.; Mondal, S.; Banerjee, R.; Bellec, A.; Garreau, Y.; Coati, A.; Chacon, C.; Girard, Y.; Lagoute, J.; Rousset, S.; et al. Importance of Epitaxial Strain at a Spin-Crossover Molecule-Metal Interface. *J. Phys. Chem. Lett.* **2019**, *10*, 4103−4109.
(23) Kelai, M.; Repain, V.; Tauzin, A.; Li, W.; Girard, Y.; Lagoute, J.; Rousset, S.; Otero, E.; Sainctavit, P.; Arrio, M.-A.; et al. Thermal Bistability of an Ultrathin Film of Iron(II) Spin-Crossover Molecules Directly Adsorbed on a Metal Surface. *J. Phys. Chem. Lett.* **2021**, *12*, 6152−6158.
(24) Railean, A.; Kelai, M.; Bellec, A.; Repain, V.; Boillot, M.-L.; Mallah, T.; Stoleriu, L.; Enachescu, C. Mechanoelastic simulations of monolayer lattices of spin crossover molecules on a substrate. *Phys. Rev. B* **2023**, *107*, No. 014304.
(25) Bairagi, K.; Bellec, A.; Fourmental, C.; Iasco, O.; Lagoute, J.; Chacon, C.; Girard, Y.; Rousset, S.; Choueikani, F.; Otero, E.; et al. Temperature-, Light-, and Soft X-ray-Induced Spin Crossover in a Single Layer of Fe^{II} -Pyrazolylborate Molecules in Direct Contact with Gold. *J. Phys. Chem. C* **2018**, *122*, 727−731.

(26) Bairagi, K.; Bellec, A.; Fourmental, C.; Tong, Y.; Iasco, O.; Lagoute, J.; Chacon, C.; Girard, Y.; Rousset, S.; Choueikani, F.; et al. Correction to Temperature-, Light-, and Soft X-ray-Induced Spin Crossover in a Single Layer of Fe^{II} -Pyrazolylborate Molecules in Direct Contact with Gold. *J. Phys. Chem. C* **2018**, *122*, 29080−29080.
(27) Tong, Y.; Kelaï, M.; Bairagi, K.; Repain, V.; Lagoute, J.; Girard, Y.; Rousset, S.; Boillot, M.-L.; Mallah, T.; Enachescu, C.; et al. Voltage-Induced Bistability of Single Spin-Crossover Molecules in a Two-Dimensional Monolayer. *J. Phys. Chem. Lett.* **2021**, *12*, 11029−11034.
(28) Giannozzi, P.; Baroni, S.; Bonini, N.; Calandra, M.; Car, R.; Cavazzoni, C.; Ceresoli, D.; Chiarotti, G. L.; Cococcioni, M.; Dabo, I.; et al. QUANTUM ESPRESSO: a modular and open-source software project for quantum simulations of materials. *J. Phys.: Condens. Matter* **2009**, *21*, 395502.
(29) Giannozzi, P.; Andreussi, O.; Brumme, T.; Bunau, O.; Buongiorno Nardelli, M.; Calandra, M.; Car, R.; Cavazzoni, C.; Ceresoli, D.; Cococcioni, M.; et al. Advanced capabilities for materials modelling with Quantum ESPRESSO. *J. Phys.: Condens. Matter* **2017**, *29*, 465901.
(30) Perdew, J. P.; Burke, K.; Ernzerhof, M. Generalized Gradient Approximation Made Simple. *Phys. Rev. Lett.* **1996**, *77*, 3865−3868.
(31) Grimme, S.; Antony, J.; Ehrlich, S.; Krieg, H. A consistent and accurate ab initio parametrization of density functional dispersion correction (DFT-D) for the 94 elements H-Pu. *J. Chem. Phys.* **2010**, *132*, 154104.
(32) Cococcioni, M.; de Gironcoli, S. Linear response approach to the calculation of the effective interaction parameters in the *LDA + U* method. *Phys. Rev. B* **2005**, *71*, No. 035105.
(33) Fahs, A.; Mi, S.; Nicolazzi, W.; Molnár, G.; Bousseksou, A. Disentangling Surface Energy and Surface/Interface Stress Effects in Spin Crossover Nanomaterials. *Advanced Physics Research* **2023**, *2*, 2200055.
(34) Mi, S.; Ridier, K.; Molnár, G.; Nicolazzi, W.; Bousseksou, A. Effects of the surface energy and surface stress on the phase stability of spin crossover nano-objects: a thermodynamic approach. *Nanoscale* **2024**, *16*, 7237−7247.
(35) Bellec, A.; Garreau, Y.; Creuze, J.; Vlad, A.; Picca, F.; Sauvage-Simkin, M.; Coati, A. Ag on a Ni vicinal surface: Coupling Stranski-Krastanov and "magic" heteroepitaxial growth. *Phys. Rev. B* **2017**, *96*, No. 085414.
(36) Zhang, K.; Hanf, M.-C.; Bernard, R.; Borensztein, Y.; Cruguel, H.; Resta, A.; Garreau, Y.; Vlad, A.; Coati, A.; Sciacca, D.; et al. The Ground State of Epitaxial Germanene on Ag(111). *ACS Nano* **2023**, *17* (16), 15687−15695.
(37) Ohresser, P.; Otero, E.; Choueikani, F.; Stanescu, S.; Deschamps, F.; Ibis, L.; Moreno, T.; Polack, F.; Lagarde, B.; Marteau, F.; et al. Polarization characterization on the DEIMOS beamline using dichroism measurements. *Journal of Physics: Conference Series* **2013**, *425*, 212007.
(38) Blöchl, P. E. Projector augmented-wave method. *Phys. Rev. B* **1994**, *50*, 17953−17979.
(39) Dudarev, S. L.; Botton, G. A.; Savrasov, S. Y.; Humphreys, C. J.; Sutton, A. P. Electron-energy-loss spectra and the structural stability of nickel oxide: An LSDA+U study. *Phys. Rev. B* **1998**, *57*, 1505−1509.

https://doi.org/10.1021/acs.jpclett.6c00550
J. Phys. Chem. Lett. 2026, 17, 5223−5230